This manuscript has been submitted to the Quarterly Journal of the Royal Meteorological Society and has not been peer-reviewed.

ORIGINAL ARTICLE

Journal Section

Dynamical controls on intensity-duration characteristics of heatwaves in an idealised model

Abel Shibu[1] | **Joy Monteiro**[1,2]

[1]Department of Earth and Climate Science, Indian Institute of Science Education and Research Pune, Pune, India

[2]Department of Data Science, Indian Institute of Science Education and Research Pune, Pune, India

Correspondence
Abel Shibu, Department of Earth and Climate Science, Indian Institute of Science Education and Research Pune, Pune, India.
Email: abels2000@gmail.com

Funding information

An idealised climate model is used to study the contribution of the atmospheric circulation to the intensity-duration characteristics of heatwaves. Using the observed correlation between near-surface temperature and lower tropospheric dry static energy (DSE), we study the energetics of the lower troposphere during heatwaves in the model. We observe that, remarkably, the intensity-duration characteristics of heatwaves are primarily controlled by zonal advection of DSE, parallel to the climatological gradient of DSE. In regions of non-zero climatological lower tropospheric winds, this leads to a phenomenon which we term as a heatwave "conveyor belt" where DSE anomalies advected by the climatological winds lead to DSE accumulation profiles which determines heatwave intensity and duration. We show that changes in intensity-duration characteristics by latitude are primarily determined by changes in the magnitude of the zonal winds. Our results propose a new, circulation focused viewpoint to study heatwave characteristics.

KEYWORDS
Heatwaves, atmospheric circulation, idealised modelling, extreme events, heatwave intensity and duration

1 | INTRODUCTION

Heatwaves are periods of extremely high near-surface temperature, and are usually defined as discrete events (or periods of time) when the exceedance of a certain threshold of two-meter temperature is observed (Perkins and Alexander, 2012). This event-based definition of heatwaves naturally leads to the question of characterizing such events, and heatwaves are typically described by their intensity-duration-frequency characteristics (Perkins and Alexander, 2012; Perkins, 2015), with intensity and duration being characteristics of individual events whereas frequency is an inter-event characteristic.

The contribution to the lifecycle of a heatwave can separated into two distinct kinds:

- Adiabatic contribution – The presence of anticyclones which lead to subsidence driven heating and the transport of heat across climatological gradients of dry static energy by the atmospheric circulation.
- Diabatic or boundary contribution – Increased sensible heat fluxes due to a combination of enhanced shortwave radiation (due to the reduction in cloudiness by the anticyclone-driven subsidence) and/or surface characteristics such as vegetation and soil moisture which could enhance sensible heat fluxes.

A large number of studies from across the world have suggested that heatwave intensity and duration is primarily controlled by the boundary contribution and feedbacks with the boundary layer, with the large-scale circulation playing a secondary role (see reviews by Perkins, 2015; Domeisen et al., 2022, and references therein). However, the precise mechanism by which the large-scale circulation could impact intensity-duration characteristics has not been, to our knowledge, systematically studied previously.

Looking at boundary contributions, soil moisture is usually considered a “slow” controlling factor that changes at the seasonal timescale, whereas cloudiness can change over the duration of a single event. In monsoonal regions like South Asia where the heatwave season is actually spring and not summer, cloudiness is at a annual minimum during the heatwave (or pre-monsoon) season, and large changes in shortwave forcing during heatwaves is unlikely. Furthermore, soil moisture is climatologically at its minimum value as well during this season. This situation opens up the possibility that the circulation could play a more important role in setting the intensity-duration characteristics of heatwaves in such regions, besides being an interesting aspect of heatwave dynamics.

As mentioned previously, the current understanding of the role of circulation focuses on transport of heat across climatological gradients, which are typically in the vertical due to the atmospheric stratification and north-south due to the meridional distribution of insolation. Quantifying the contribution of circulation related controls to heatwave characteristics in observations is challenging due to the strong influence of the boundary in determining near-surface temperatures. One potential way forward is to use idealised models where the boundary effects are less important (Jiménez-Esteve et al., 2022; Jiménez-Esteve and Domeisen, 2022). Furthermore, since temperature is not conserved by the circulation, quantifying the contribution of individual (zonal/meridional/vertical) components of the circulation to either intensity or duration of heatwaves (which is measured primarily by near-surface temperature) becomes problematic.

In this study, we use an idealised climate model which is configured to reduce boundary effects on heatwaves and study the contribution of the circulation to the lower-tropospheric dry static energy (DSE) budget. Since DSE is conserved by the flow, it is possible to quantify the contribution of the individual components of the circulation in an unambiguous manner. By relating DSE to near-surface temperature, we are then able to develop a quantitative framework to partition intensity and duration contributions into the individual components of the circulation. We choose to focus on the energetics of heatwaves rather than the mechanisms since, as we will see, heatwave energetics

provide al alternate perspective to study heatwave dynamics from. In particular, we aim to develop a framework to quantify the contributions of individual components of the circulation to the intensity and duration characteristics of heatwaves in the idealised model, and how these contributions change with latitude.

2 | METHODS

2.1 | Model description

For this study, we use an idealised general circulation model (GCM) created using the climt modelling toolkit (Monteiro et al., 2018). Our GCM configuration is similar to the model setup in (Frierson et al., 2006). To summarise, our model has a slab ocean, with zonally symmetrical strips of land between 20° and 60° in both hemispheres. The area type is either land or sea, with different depth and heat capacity values for sea and land grids. The prescribed depth value for land is 1 m, with a heat capacity value of 2000 $\mathrm{Jkg^{-1}K^{-1}}$. For the ocean, the prescribed depth value is 2 m, with the heat capacity being the heat capacity of water, 4182 $\mathrm{Jkg^{-1}K^{-1}}$. The temperature of the surface is controlled dynamically by the energy balance at the surface. There is no topography in our model. The model also does not have clouds or sea ice. A grey radiation scheme is used, with values for atmosphere opacity τ prescribed as

$$\tau = [\tau_{0e} + (\tau_{0p} - \tau_{0e}) \sin^2(\phi)](\frac{p}{p_s}) \tag{1}$$

where $\tau_{0p} = 1.5$ and $\tau_{0e} = 6$ are values of atmosphere opacity at the surface at the pole and equator, respectively. p and p_s are pressure and surface pressure respectively and ϕ is the latitude. The vertical profile of optical depth with pressure in our model is linear, unlike in Frierson et al. (2006), where a combination of linear and quartic terms were used. The incoming solar flux values R_s has an off-equatorial maximum, with maximum flux at 10°N, and decreasing towards the poles with functional form

$$R_s(\phi) = \begin{cases} R_{max}[1 + \Delta_s p_2(\phi - 10^{\circ})] & \text{for } \phi \geq -80^{\circ} \\ R_{max}[1 + \Delta_s p_2(-90^{\circ})] & \text{otherwise} \end{cases} \tag{2}$$

where $p_2(\theta) = \frac{1}{4}[1 - 3\sin^2\theta]$ is the second Legendre polynomial and ϕ is the latitude. $R_{max} = 150$ $\mathrm{Wm^{-2}}$ and $\Delta_s = 1.4$ controls the meridional gradient of solar flux. The model has no seasonality and no diurnal cycle. Moist convection in the model is parameterized using the Emanuel convection scheme (Emanuel and Živković Rothman, 1999). The surface flux and boundary layer formulation is as in Frierson et al. (2006). The relative humidity at the surface is set to the saturation specific humidity at the surface temperature. However, for the land grids, we scale the relative humidity at the surface by a parameter $S_L = 0.7$. This parameter models the moisture limitation over land and controls the ratio of Sensible Heat Flux (SHF) to Latent Heat Flux (LHF).

A spectral dynamical core solves the primitive equations and is run at T42 grid resolution (64 x 128, 2.76° x 2.79°), which equates to a grid length of approximately 310 km at the equator. The model has 28 height levels and an integration time step of 20 minutes. This model was run for a duration of 1000 years and the model variables are saved as a daily average for each day. The spinup time of the model, the time for the model's climate to equilibrate, is around a year. We have spun up the model for 3 years to ensure that equilibrium was reached.

| Model climatology

The 30-year climatology of our model is shown in Fig. 1. As the maximum insolation is at 10°N, the temperature maximum is in the northern hemisphere (Fig. 1, panel a and b). The jet streams are clear in the zonally averaged zonal wind plot (panel c), with a stronger jet in the winter hemisphere as expected. The jet in the northern hemisphere is at 54.4°N, over the poleward land region, while the jet in the southern hemisphere is at 26.5°S. The maximum jet speed in the northern hemisphere is 27 ms^{-1}, and 51 ms^{-1} the southern hemisphere. The maximum of the storm track intensity, indicated by the zonal mean variance of the meridional wind (panel d) is close to the zonal jet maximum, atleast in the northern hemisphere. The average sensible and latent heat fluxes over land are 8.15 Wm^{-2} and 47.91 Wm^{-2}.

2.2 | Heatwaves

Since we are interested in the intensity-duration characteristics of heatwaves and their relationship to the circulation, we have studied four different patches of land of dimensions around 10°x10°(lat x lon), centred at around 35N, 40N, 45N and 50N (see Fig. 1, panel b). In Fig. 1, the land patches are shown at different longitudinal locations for clarity, the land patches are actually at the same longitudinal location (100°-110°). Moreover, as the model is zonally symmetric, the zonal position does not make a difference. The size of the patches are of the order of the synoptic scale (more than 1000km) to specifically study large-scale processes.

We calculate and store T_a, the daily average of the spatial average of lowest-level model temperature over the land patches of interest. The 95th percentile of the T_a distribution, T_{95}, is set to be the heatwave threshold. To calculate the intensity and duration of heatwaves from the daily averaged temperature data, we use linear interpolation to identify the approximate (sub-daily) time where the heatwave threshold is crossed and to estimate the temperature across the heatwave duration. T_{95} is computed separately for each land patch.

Heatwave definition and characteristics

We define heatwaves as any continuous period of three or more days during which T_a exceeds T_{95} in a land patch. The duration of a heatwave is the continuous period over which T_a exceeds T_{95}. From our heatwave definition, the minimum duration possible is 3 days. Two heatwaves separated by even only a day with T_a below T_{95} are still considered as two separate events. The intensity of a heatwave is defined as the mean difference between T_a and T_{95} across its duration. For this study, we divide the heatwaves sampled into four classes - high intensity, low intensity, high duration and low duration heatwaves. The high intensity and high duration classes consist of heatwaves whose respective attributes are higher than their 90th percentile value across all heatwaves. Similarly, the low intensity and low duration classes contain heatwaves whose respective attributes are lower than their 10th percentile value across all heatwaves.

Fig. 2 shows the intensity-duration distribution for the land patch centered at 45N. Fig. 3 shows how the average intensity/duration values for the top and bottom 10 percentile heatwaves change across the different land locations. We see that as we move from the northernmost land towards the equator, the average intensity values of both the top and bottom 10 percentile heatwaves decreases, by around 41% and 44% respectively. In contrast, as we move from the northernmost land towards the equator, changes in heatwave duration occurs primarily in the positive tail of the duration distribution. The average duration of the top 10 percentile heatwaves increase by around 28%, while the average duration of the bottom 10 percentile heatwaves does not exhibit any clear change. The relatively fixed duration values for low duration heatwaves could be due to the 3-day minimum duration constraint, and the relative

abundance of short heatwaves.

2.3 | Heatwave energetics

To study the energetics of heatwaves, we move from a framework of temperature to that of energy. We find that during heatwave days, there is a strong correlation between the average lowest-level air temperature over the area of interest and the total dry static energy (DSE) over the same horizontal area, from the surface upto 850hPa (Fig. 4, panel a). This correlation is robust across the various land locations, and enables us to understand temperature extremes in terms of DSE, which is conserved in the absence of diabatic sources. In this and subsequent analyses, we include one day before and after the heatwave event. This allows us to also capture the processes that push temperatures across the heatwave threshold in both directions.

We observe that the sensible heat flux during heatwaves over the area of interest is negative (Fig. S1 in the supplementary material), suggesting a warmer atmosphere during heatwaves. This observation is robust across land locations. This allows us rule out the possibility of enhanced surface fluxes being a forcing mechanism for heatwaves in this model. Conversely, this observation strongly suggests that the heatwaves in this model are primarily forced by the circulation, with sensible heat flux only acting as a negative response to this forcing.

Across land locations, for heatwave periods, we find that changes in the total DSE upto 850hPa can be explained to a large extent (except for a few outliers) by the DSE convergence in the atmosphere alone (Fig. 4, right panel). From Fig. 4, we see that the linear fit is slightly steeper than the 1:1 line, with the predicted rate slightly overestimating the actual rate. This bias is consistent with the fact that we have excluded surface flux and other components like radiative forcing, which act as a sink of DSE.

We calculate convergence in the area of interest for heatwave periods using the daily-averaged model variables. The model variables are linearly interpolated to uniform pressure levels from 970hPa to 290hPa, at 20hPa intervals. The model does not output vertical winds, and we calculate it from the horizontal winds using the relation $\boldsymbol{\nabla}.\vec{\mathbf{u}} = 0$ since the primitive equations are incompressible.

DSE (denoted by S from here onwards) at each pressure level is calculated using the relation $S{=}c_pT{+}gz$, where c_p=1004.64 J kg^{-1} K^{-1} is the specific heat of air at constant pressure, T is temperature, g= 9.80665 ms^{-2} is acceleration due to gravity, and z is height above the surface.

DSE convergence -$\boldsymbol{\nabla}.(S\vec{\mathbf{u}})$ can be written as

$$-\boldsymbol{\nabla}\left(S\vec{\mathbf{u}}\right) = -(\vec{\mathbf{u}}.\boldsymbol{\nabla}(S) + S(\boldsymbol{\nabla}.\vec{\mathbf{u}})) \tag{3}$$

Since the flow is incompressible, the second term of Eqn. 3 is zero, and DSE convergence is just -$\vec{\mathbf{u}}.\boldsymbol{\nabla}(S)$. This implies that only the DSE advection terms can cause any DSE accumulation, and hereon we work with DSE advection instead of DSE convergence. Henceforth, for compactness, we also omit the negative sign for all mentions of advection terms in the text. However, calculations of the advective terms have included the negative sign.

2.4 | Reynolds decomposition

To understand how the different advective process components govern intensity and duration of heatwaves, we perform a Reynolds decomposition of the DSE forcing $\vec{\mathbf{u}}.\boldsymbol{\nabla}(S)$ within the area of interest, from the surface upto 850hPa. We split $\vec{\mathbf{u}}$ into its mean and anomaly components as $\vec{\mathbf{u}} = \overline{\vec{\mathbf{u}}} + \vec{\mathbf{u}}'$. Similarly, we split DSE as $S = \overline{S} + S'$. Since the model

has a constant forcing without diurnal or seasonal cycles, we set the mean values to be the 1000 year means from the long model run. The DSE forcing $\vec{\mathbf{u}}.\boldsymbol{\nabla}(S)$ can be written as

$$\vec{\mathbf{u}}.\boldsymbol{\nabla}(S) = \overline{\vec{\mathbf{u}}}.\boldsymbol{\nabla}\left(\overline{S}\right) + \overline{\vec{\mathbf{u}}}.\boldsymbol{\nabla}(S') + \vec{\mathbf{u}}'.\boldsymbol{\nabla}\left(\overline{S}\right) + \vec{\mathbf{u}}'.\boldsymbol{\nabla}(S') \tag{4}$$

Given the zonal symmetry of the model, we expect the $\frac{\partial \overline{S}}{\partial x}$ to be close to zero. We also expect $\overline{v}$ to be small. Conversely, terms containing v' and $\overline{u}$ (depending on proximity to the jet stream), could be important.

2.5 | Intensity-duration control

Heatwave intensity can be calculated from the total DSE forcing by reconstructing the magnitude of DSE accumulation across time. This calculation can also be performed separately for the various DSE forcing components to estimate their individual intensity contributions (See Figs. 13 and 14). As this operation is linear, the intensity contributions of the different components add up to give the total intensity of the heatwave.

To quantify the contribution of different processes to heatwave duration, we have plotted the average magnitude associated with each process on the n^{th} day after heatwave start. (See Figs. 15 and 16). As we intend to capture the trends in the accumulation profiles of various components in relation to heatwave duration, we do not normalise on duration. We compute the average accumulation rates associated with each process across heatwaves that have survived till the n^{th} day. This enables us to understand their temporal profiles and trends with heatwave duration.

3 | RESULTS

3.1 | Low-level DSE advection

In Fig. 5, we have plotted the total DSE advection within the boxes centered at 50N and 35N, from the surface upto 850hPa. To compare between heatwaves of varying lengths, we have plotted against time fraction, with 0 and 1 being the first and last day across all heatwaves. As we would expect, DSE advection is initially positive, leading to an accumulation of DSE. Advection then reduces to zero (at heatwave maximum), before reversing sign. Negative DSE advection towards the end of the heatwave ventilates the accumulated DSE, ending the event.

We see from Fig. 5 that intense heatwaves are associated with a high amplitude of positive and negative DSE advection, with an almost linear profile. In contrast, high duration heatwaves have a persistent rate of accumulation, with a brief and delayed ventilation. Interestingly, the DSE advection pattern of low intensity heatwaves looks similar to that of high duration heatwaves, and that of low duration heatwaves looks like that of high intensity heatwaves. These patterns are consistent across all land locations (Not shown). It is important to note that the amplitude of DSE advection decreases from the 50N box to the 35N box, across all heatwave classes. This explains why the average intensity of heatwaves also decreases in the same direction.

3.2 | Reynolds components

We observe that of all the terms obtained from Reynolds decomposition at the lower levels (surface to 850hPa), four horizontal terms and the vertical components account for just about all of DSE advection. The horizontal terms are

- $v' \frac{\partial \overline{S}}{\partial y}$ - meridional advection of mean DSE by anomalous wind
- $v' \frac{\partial S'}{\partial y}$ - meridional advection of anomalous DSE by anomalous wind
- $\overline{u} \frac{\partial S'}{\partial x}$ - zonal advection of anomalous DSE by mean wind
- $u' \frac{\partial S'}{\partial x}$ - zonal advection of anomalous DSE by anomalous wind

Fig. S2 in the supplementary material shows the lifetime profiles reconstructed from the four horizontal terms and the vertical terms, and are almost indistinguishable from the total lifetime DSE advection profiles in Fig. 5. The lifetime profiles of the horizontal components across different land locations are shown below. We have drawn these plots for high intensity and high duration heatwave classes separately (Fig. 6, 7, 8, and 9). The vertical component is an order of magnitude smaller than the horizontal components, and has been omitted in the plots.

We see that even though components have different lifetime profiles between the high intensity and high duration classes, for a given class most components do not change significantly in magnitude or profile across the different land locations. Specifically, the climatological DSE gradient does not change much across land patches (See Fig. S4 in the supplementary material), suggesting that the mixing length does not change across land patches. The only component that systematically changes in magnitude across land locations is the $\overline{u} \frac{\partial S'}{\partial x}$ component, which decreases sharply as we move equatorward, away from the surface westerlies.

Comparing between Fig. 7 and 9, we also see that the lifetime profiles of $\overline{u} \frac{\partial S'}{\partial x}$ for high intensity and high duration heatwaves are very similar to the total DSE advection profiles (Fig. 5). For intense heatwaves, $\overline{u} \frac{\partial S'}{\partial x}$ changes linearly from accumulation to ventilation (same as negative accumulation), while long duration heatwaves have a persistent accumulation phase followed by a short and delayed ventilation phase. These observations suggest that the $\overline{u} \frac{\partial S'}{\partial x}$ term in particular is responsible for the trends in intensity-duration characteristics across land locations.

3.3 | Vertical DSE profiles

We have separately plotted the mean accumulation and ventilation profiles for high vs low heatwave intensity and duration (Fig. 10). These plots are for the land patch centered at 45N. However, these profiles are qualitatively similar across the different land locations.

For the heatwave intensity classes (Fig. 10, Top panels), the main difference between high and low intensity heatwaves is the magnitude of low-level accumulation. Intense heatwaves have much higher low-level accumulation than low intensity heatwaves. The larger accumulation in intense heatwaves is also followed by a large ventilation across the vertical. The large accumulation rate in intense heatwaves allows them to quickly reach temperatures much higher than the heatwave threshold. When this accumulation phase is followed by a strong ventilation phase, temperatures quickly drop to below the threshold. The short accumulation and ventilation phases ensure that these heatwaves spends most of their duration close to their maximum temperatures, resulting in intense heatwaves.

For the duration classes (Fig. 10, Bottom panels), the accumulation pattern for high and low duration heatwaves do not seem very different, and mean accumulation is slightly smaller for long heatwaves only at the lower levels. However, we see that high duration heatwaves are accompanied by much weaker ventilation across the vertical in comparison to low duration heatwaves. This ventilation profile seems to be a predominant factor associated with heatwave duration since it delays the ventilation of the accumulated DSE.

In Figs. 11 and 12, we have plotted the mean vertical accumulation and ventilation profiles for the various horizontal components. We see that the $v' \frac{\partial \overline{S}}{\partial y}$ component contributes predominantly to accumulation across the vertical, and provides negligible ventilation. In contrast, the $v' \frac{\partial S'}{\partial y}$ component is responsible for much of the ventilation, and does not provide significant accumulation. The $v' \frac{\partial \overline{S}}{\partial y}$ term advects the climatological DSE into the box, while the

$v' \frac{\partial S'}{\partial y}$ term advects the resultant DSE anomaly away from the box (see Fig. S3 in the supplementary material). These meridional terms are much larger than the zonal terms, and the accumulation from $v' \frac{\partial \overline{S}}{\partial y}$ almost balances the ventilation provided by $v' \frac{\partial S'}{\partial y}$, atleast close to the surface. Above 800hPa, the accumulation from $v' \frac{\partial \overline{S}}{\partial y}$ is more than the ventilation provided by $v' \frac{\partial S'}{\partial y}$. The zonal terms, $\overline{u} \frac{\partial S'}{\partial x}$ and $u' \frac{\partial S'}{\partial x}$ provide both accumulation and ventilation close to the surface. Above 800hPa however, both zonal terms provide more ventilation than accumulation. This imbalance somewhat counteracts the difference between accumulation and ventilation in the meridional terms above 800hPa.

For high intensity heatwaves, we see that the DSE accumulation from $v' \frac{\partial \overline{S}}{\partial y}$ is larger in comparison to low intensity heatwaves. This is expected, as this is the primary accumulation term, and as higher heatwave intensity implies higher DSE accumulation. In contrast, the ventilation provided by $v' \frac{\partial S'}{\partial y}$ does not vary between heatwave classes. The ventilation from $v' \frac{\partial S'}{\partial y}$ is also slighlty lower than the accumulation provided by $v' \frac{\partial \overline{S}}{\partial y}$ at the lowest levels. This discrepancy in DSE is made up for by $\overline{u} \frac{\partial S'}{\partial x}$ and $u' \frac{\partial S'}{\partial x}$, with both providing more ventilation for high intensity heatwaves.

Between the high and low duration classes, we see that both the accumulation provided by $v' \frac{\partial \overline{S}}{\partial y}$ and the ventilation provided by $v' \frac{\partial S'}{\partial y}$ are very similar. However, at the lowest levels, there is a discrepancy between the accumulation and ventilation provided by these terms, with accumulation being slightly larger than ventilation. This difference is balanced by $\overline{u} \frac{\partial S'}{\partial x}$ and $u' \frac{\partial S'}{\partial x}$, but at different rates for high and low duration heatwaves. Low duration heatwaves are associated with a higher rate of ventilation in the zonal components. In contrast, in high duration heatwaves, these components provide ventilation at a lower rate.

3.4 | Contribution to Intensity

In Figs. 13 and 14, we have plotted the intensity contributions associated with different processes for the top and bottom 10 percentile intensity classes, respectively. For completeness, we have also computed the residual term as the deviation between the actual DSE difference and DSE advection (As in Fig. 4). This term includes processes that we have not accounted for like surface fluxes and radiation forcing, along with averaging-related errors.

We have converted quantities in these plots from Joules to Kelvin using the linear relationship between low-level DSE and lowest-level model temperature (see Fig. 4). Note that the mean total intensities we have calculated from the DSE forcing in Figs. 13 and 14 are in close agreement with their corresponding values in Fig. 3.

In subsequent analyses, we have combined the $v' \frac{\partial \overline{S}}{\partial y}$ and $v' \frac{\partial S'}{\partial y}$ terms as $v' \frac{\partial S}{\partial y}$. The $v' \frac{\partial \overline{S}}{\partial y}$ term is predominantly accumulating and the $v' \frac{\partial S'}{\partial y}$ is ventilating. The combination of these terms ($v' \frac{\partial S}{\partial y}$) explains trends in heatwave characteristics better than either term individually.

Figs. 13 and 14 highlights the components responsible for the difference in mean intensity between the top and bottom intensity classes, and between extreme land locations. Between the top and bottom intensity classes, the component that shows the most systematic change in intensity contribution is $v' \frac{\partial S}{\partial y}$. Between extreme land locations however, the $\overline{u} \frac{\partial S'}{\partial x}$ term has the most significant difference in contribution. Away from the jet, the magnitude of the $\overline{u} \frac{\partial S'}{\partial x}$ is too small to have any significant contribution to intensity.

The residual term shows some differences between intensity classes and land locations. However, the trends in the residual term is always opposed to that of intensity and in all cases, the residual term only contributes negatively to heatwave intensity. This observation is in agreement with our understanding that the processes in the residual term only act to dampen heatwaves.

3.5 | Contribution to Duration

The duration of heatwaves is considered to be the time taken for the DSE to rise above and fall below its threshold value. This requires the initial accumulation of DSE (intiating the heatwave) followed by ventilation of DSE (dissipating the heatwave).

We have plotted the average accumulation rates associated with different components across the duration of the event. We have plotted this separately for the top and bottom 10 percentile duration classes for the extreme land locations (Figs. 15 and 16).

In Figs. 15 and 16, we have only shown the major terms ($v' \frac{\partial S}{\partial y}$, $\overline{u} \frac{\partial S'}{\partial x}$, $u' \frac{\partial S'}{\partial x}$ and the residual). However, the total accumulation profiles also contains the vertical term, which we have not shown due to it's relatively small contribution.

The most systematic difference between the top and bottom duration classes is the number of days before ventilation (same as negative accumulation) starts. In the top duration class, ventilation starts after around 6 days, whereas it only takes about 1.5 days in the bottom duration class. Another difference is the ventilation provided by the $v' \frac{\partial S}{\partial y}$ term. The $v' \frac{\partial S}{\partial y}$ term contributes to ventilation in the bottom duration class, leading to a shorter duration of heatwaves. For the top duration class, this term provides relatively negligible ventilation.

The primary ventilation term is different between extreme land locations. Close to the jet, ventilation follows the $\overline{u} \frac{\partial S'}{\partial x}$ term, and away from the jet, it follows the $u' \frac{\partial S'}{\partial x}$ term. These processes have different ventilation rates, with $\overline{u} \frac{\partial S'}{\partial x}$ being stronger than $u' \frac{\partial S'}{\partial x}$. Given that relevant accumulation characteristics stay the same across extreme land locations, the change in ventilation terms and associated rates is responsible for the duration trend across land locations. Moreover, we see that the average ventilation provided by the $\overline{u} \frac{\partial S'}{\partial x}$ term is strongly linear with $\overline{u}$ (Fig. S5 in the supplementary material). This implies that ventilation across land locations is governed primarily by the zonal wind velocity, $\overline{u}$ for the $\overline{u} \frac{\partial S'}{\partial x}$ term and u' for the $u' \frac{\partial S'}{\partial x}$ term. As $\overline{u}$ close to the jet stream has a constant direction and is generally of higher magnitude than u', which varies in both direction and magnitude with time, this observation also explains why $\overline{u} \frac{\partial S'}{\partial x}$ provide more ventilation than $u' \frac{\partial S'}{\partial x}$ on average.

We can estimate heatwave duration from the total accumulation profiles in Fig. 15 and 16 by first dividing the profile into accumulation and ventilation phases, and then calculating the ventilation time that would be needed to balance the total accumulation. Heatwave duration can be calculated as the sum of the number of days of accumulation and the ratio of total accumulation to mean ventilation. The duration estimate from this calculation agrees very well with their corresponding values and trends in Fig. 3.

In all cases, the residual term only provides negative accumulation during the accumulation phase of heatwaves, and does not change the results much.

4 | SUMMARY AND DISCUSSION

In this study, we use an idealised GCM to better quantify the role of the atmospheric circulation in the energetics of heatwaves. We observe that winds crossing climatological DSE gradients (the meridional components) play a role in both DSE accumulation and ventilation, but cannot explain the observed DSE lifecycles. In this framework, heatwave intensity is equivalent to mean accumulation of anomalous DSE in a location during a heatwave, and heatwave duration is equivalent to the time taken to accumulate and later ventilate anomalous DSE.

Using an observed nearly-linear relationship between temperature at the lowest model level and DSE between the surface and 850 hPa, we develop a framework to quantitatively partition contributions to intensity and duration of heatwaves to different components of the circulation.

An analysis of the lifecycle of the total anomalous DSE leads to the counterintuitive observation that the winds

along climatological DSE gradients (the zonal components in our case) advecting anomalous DSE play a first-order role in shaping intensity and duration in the model. In regions of surface westerlies the zonal terms essentially amount to a translation of a two-dimensional DSE anomaly by the climatological mean zonal winds. We term this situation a "heatwave conveyor belt", since the heatwave characteristics depend on what an Eulerian observer would perceive at a given location as the DSE anomaly sweeps by. The intensity-duration characteristics in this situation depend only on the geometric properties (the zonal gradient is responsible for intensity, for instance) of the DSE anomaly. Away from the region of climatological mean surface zonal winds, the eddy winds are responsible for shaping heatwave characteristics, and due to their smaller amplitude and more complex lifecycle, lead to lower intensity and longer duration – as if the conveyor belt operator is stochastic. This mechanism of flow-based control of heatwave characteristics has (to our knowledge) not been reported previously.

Our DSE-based framework allows us to provide a quantitative partitioning of the average intensity and duration of not only individual events but a particular class of heatwaves: we had chosen high or low intensity/duration classes, but in principle any class could be chosen. Since we also account for a residual term, this framework could also incorporate surface and radiative fluxes, and could potentially be used in observational studies if such relationships are observed in the real world. Currently approaches such as model experiments or multilinear regression are used (see Arblaster et al., 2014; Wehrli et al., 2019; Miralles et al., 2014, for example), which aim to directly predict temperature rather than DSE.

From a more theoretical perspective, our results suggest that mean-eddy interactions are insufficient to recover heatwave statistics since the eddy-eddy term $v' \frac{\partial S'}{\partial y}$ plays an important role in the energy budget of heatwaves in our model. Therefore, even though quasilinear models of atmospheric macroturbulence – which ignore eddy-eddy interactions – have been successful in recovering flow statistics in a variety of geophysical flows (particularly in regions with a strong mean flow) (Schneider and Walker, 2006; Chemke and Kaspi, 2016; Delsole and Farrell, 1996; Marston and Tobias, 2023; Svirsky et al., 2023a,b), our results suggest that the ability of such models to reproduce the tails of atmospheric variability needs to be examined more closely.

We have provided a comprehensive picture of the energetics of heatwaves in our model. However, the dynamical basis of the observed patterns of DSE remains to be explored, and provides a promising avenue for future research. Adding further complexities such as stationary waves due to topography or land-sea contrast could also shed light on how such modifications changes the energetics of heatwaves, and will hopefully provide a way to better characterize the role of circulation in the dynamics of heatwaves in the real world.

code availability

The analysis code is available at `https://github.com/Ai33L/Heatwave_dyn1`

data availability

The data that support the findings of this study are available from the corresponding author upon reasonable request.

acknowledgements

The support and the resources provided by 'PARAM Brahma Facility' under the National Supercomputing Mission, Government of India at the Indian Institute of Science Education and Research (IISER) Pune are gratefully acknowledged. JMM acknowledges useful discussions with Vishal Dixit and Nili Harnik. A.S thanks Sarathchandran J. for

technical help with the supercomputer code.

conflict of interest

The authors declare no conflict of interest.

references

Arblaster, J. M., Lim, E.-P., Hendon, H. H., Trewin, B. C., Wheeler, M. C., Liu, G. and Braganza, K. (2014) Understanding Australia's hottest September on record.

Chemke, R. and Kaspi, Y. (2016) The Effect of Eddy–Eddy Interactions on Jet Formation and Macroturbulent Scales. *Journal of the Atmospheric Sciences*, **73**, 2049–2059. URL: https://journals.ametsoc.org/view/journals/atsc/73/5/jas-d-15-0375.1.xml. Publisher: American Meteorological Society Section: Journal of the Atmospheric Sciences.

Delsole, T. and Farrell, B. F. (1996) The Quasi-Linear Equilibration of a Thermally Maintained, Stochastically Excited Jet in a Quasigeostrophic Model. *Journal of the Atmospheric Sciences*, **53**, 1781–1797. URL: https://journals.ametsoc.org/view/journals/atsc/53/13/1520-0469_1996_053_1781_tqleoa_2_0_co_2.xml. Publisher: American Meteorological Society Section: Journal of the Atmospheric Sciences.

Domeisen, D. I. V., Eltahir, E. A. B., Fischer, E. M., Knutti, R., Perkins-Kirkpatrick, S. E., Schär, C., Seneviratne, S. I., Weisheimer, A. and Wernli, H. (2022) Prediction and projection of heatwaves. *Nature Reviews Earth & Environment*, **4**, 36–50. URL: https://www.nature.com/articles/s43017-022-00371-z.

Emanuel, K. A. and Živković Rothman, M. (1999) Development and Evaluation of a Convection Scheme for Use in Climate Models. *Journal of the Atmospheric Sciences*, **56**, 1766–1782. URL: http://journals.ametsoc.org.ezp.sub.su.se/doi/abs/10.1175/1520-0469(1999)056%3C1766%3ADAEOAC%3E2.0.CO%3B2. 00553.

Frierson, D. M. W., Held, I. M. and Zurita-Gotor, P. (2006) A Gray-Radiation Aquaplanet Moist GCM. Part I: Static Stability and Eddy Scale. *Journal of the Atmospheric Sciences*, **63**, 2548–2566. URL: http://journals.ametsoc.org/doi/abs/10.1175/JAS3753.1.

Jiménez-Esteve, B., Kornhuber, K. and Domeisen, D. I. V. (2022) Heat Extremes Driven by Amplification of Phase-Locked Circumglobal Waves Forced by Topography in an Idealized Atmospheric Model. *Geophysical Research Letters*, **49**, e2021GL096337. URL: https://onlinelibrary.wiley.com/doi/abs/10.1029/2021GL096337. _eprint: https://onlinelibrary.wiley.com/doi/pdf/10.1029/2021GL096337.

Jiménez-Esteve, B. and Domeisen, D. I. (2022) The role of atmospheric dynamics and large-scale topography in driving heatwaves. *Quarterly Journal of the Royal Meteorological Society*, **148**, 2344–2367. URL: https://rmets.onlinelibrary.wiley.com/doi/10.1002/qj.4306.

Marston, J. B. and Tobias, S. M. (2023) Recent Developments in Theories of Inhomogeneous and Anisotropic Turbulence. *Annual Review of Fluid Mechanics*, **55**, 351–375. URL: https://www.annualreviews.org/content/journals/10.1146/annurev-fluid-120720-031006. Publisher: Annual Reviews.

Miralles, D. G., Teuling, A. J., van Heerwaarden, C. C. and Vilà-Guerau de Arellano, J. (2014) Mega-heatwave temperatures due to combined soil desiccation and atmospheric heat accumulation. *Nature Geoscience*, **7**, 345–349. URL: https://www.nature.com/articles/ngeo2141. Publisher: Nature Publishing Group.

Monteiro, J. M., McGibbon, J. and Caballero, R. (2018) sympl (v. 0.4.0) and climt (v. 0.15.3) – towards a flexible framework for building model hierarchies in Python. *Geoscientific Model Development*, **11**, 3781–3794. URL: https://www.geosci-model-dev.net/11/3781/2018/.

Perkins, S. E. (2015) A review on the scientific understanding of heatwaves—Their measurement, driving mechanisms, and changes at the global scale. *Atmospheric Research*, **164-165**, 242–267. URL: https://www.sciencedirect.com/science/article/pii/S0169809515001738.

Perkins, S. E. and Alexander, L. V. (2012) On the Measurement of Heat Waves. *Journal of Climate*, **26**, 4500–4517. URL: https://journals.ametsoc.org/doi/abs/10.1175/JCLI-D-12-00383.1.

Schneider, T. and Walker, C. C. (2006) Self-Organization of Atmospheric Macroturbulence into Critical States of Weak Nonlinear Eddy–Eddy Interactions. *Journal of the Atmospheric Sciences*, **63**, 1569–1586. URL: http://journals.ametsoc.org/doi/abs/10.1175/jas3699.1.

Svirsky, A., Herbert, C. and Frishman, A. (2023a) Statistics of inhomogeneous turbulence in large-scale quasigeostrophic dynamics. *Physical Review E*, **108**, 065102. URL: https://link.aps.org/doi/10.1103/PhysRevE.108.065102.

— (2023b) Two-Dimensional Turbulence with Local Interactions: Statistics of the Condensate. *Physical Review Letters*, **131**, 224003. URL: https://link.aps.org/doi/10.1103/PhysRevLett.131.224003.

Wehrli, K., Guillod, B. P., Hauser, M., Leclair, M. and Seneviratne, S. I. (2019) Identifying Key Driving Processes of Major Recent Heat Waves. *Journal of Geophysical Research: Atmospheres*, **124**, 11746–11765. URL: https://onlinelibrary.wiley.com/doi/abs/10.1029/2019JD030635. _eprint: https://onlinelibrary.wiley.com/doi/pdf/10.1029/2019JD030635.

List of Figures

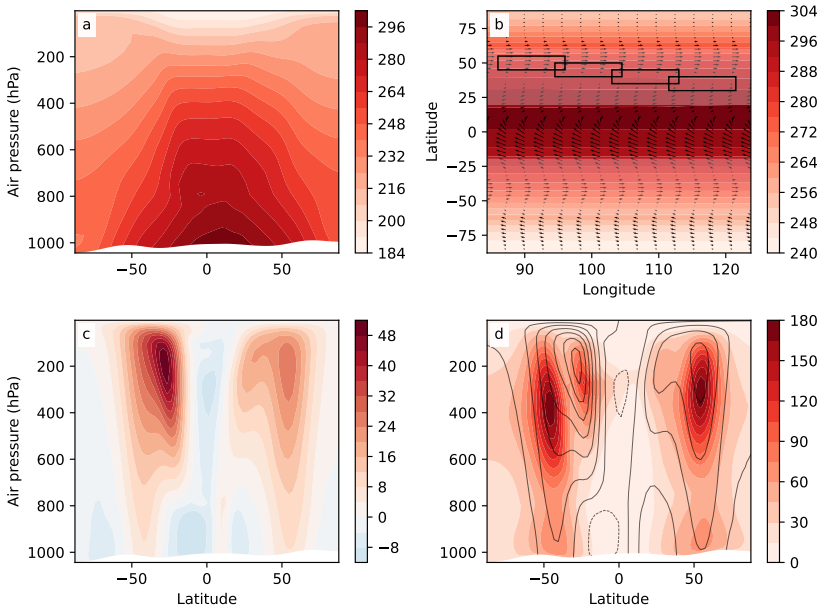

FIGURE 1 Model climatology. (a) Zonally averaged air temperature (K). (b) Lowest level winds (ms^{-1}) overlaid on lowest level air-temperature (K). The location and extent of land in the model is depicted by the light shading, and the land patches of interest are depicted by solid boxes. All land patches are between 100-110 longitude, boxes in the plot have been separated for clarity. (c) Zonally averaged zonal winds (ms^{-1}). (d) Zonal mean variance of meridional wind (m^2s^{-2}) - marks the location of the storm track. The zonally averaged zonal wind is overlaid (black contours).

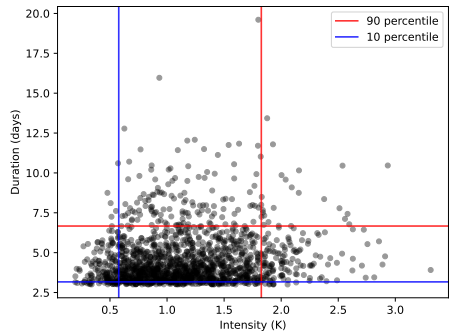

FIGURE 2 Scatter plot of heatwave intensity-duration for land patch centered at 45N. The red and blue lines indicate the 90 and 10 percentile thresholds for intensity and duration.

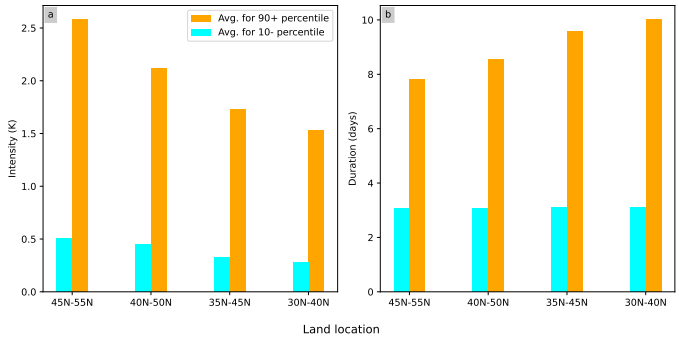

FIGURE 3 Average intensity/duration values for the lowest and highest 10 percentile heatwaves across land locations. (a) Intensity values. (b) Duration values.

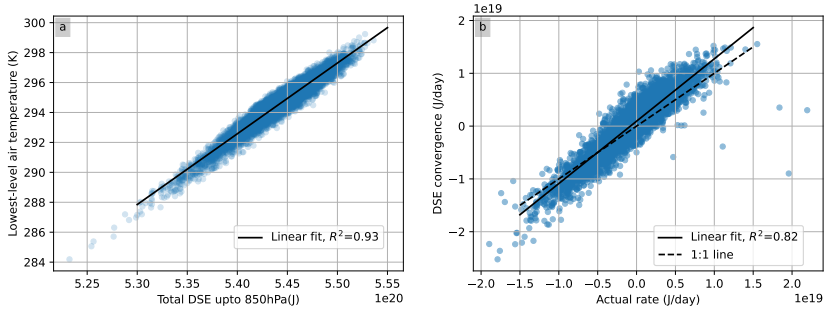

FIGURE 4 (a) Correlation between average air-temperature and total DSE for the land centered at 45N. The blue dots are the actual values, the black line is a linear fit. (b) Comparison between actual rate of dse change and the rate predicted by DSE convergence alone during heatwave periods for the land centered at 45N. DSE is integrated from the surface upto 850hPa. The slope of the linear fit is 1.18.

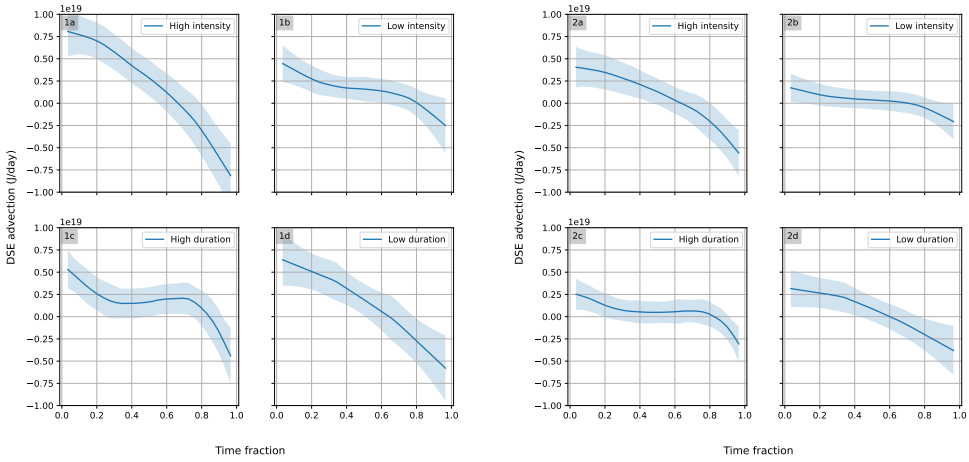

FIGURE 5 Total low-level lifetime DSE advection profiles for the different intensity and duration classes. Plots on the left (1a-1d) are for the land patch centered at 50N and plot on the right (2a-2d) are for the land patch centered at 35N. To compare between heatwaves of varying lengths, we have plotted against time fraction, with 0 and 1 being the first and last day across heatwaves. The lines represent the mean, and shading shows standard deviation across heatwaves. Left - land patch centered at 50N. Right - land patch centered at 35N.

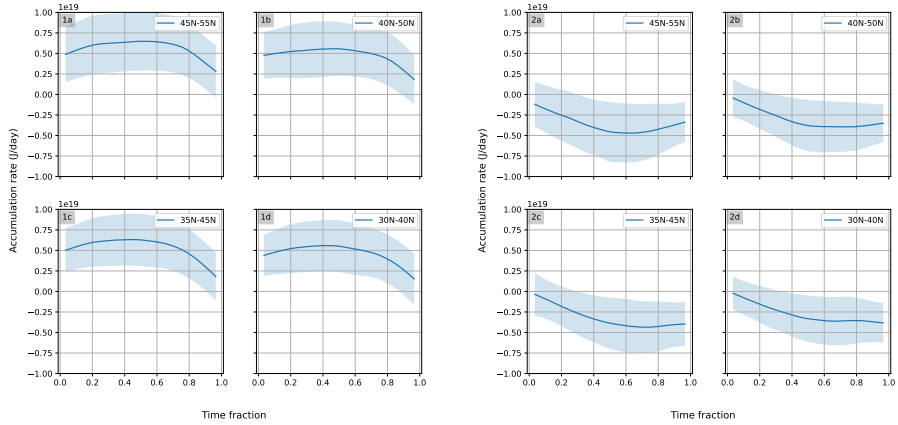

FIGURE 6 Lifetime profiles of $v' \frac{\partial \overline{S}}{\partial y}$ (1a-1d) and $v' \frac{\partial S'}{\partial y}$ (2a-2d) for high intensity heatwaves across land locations. These are plotted against time fraction, with 0 and 1 being the first and last day across heatwaves. The lines represent the mean, and shading shows standard deviation across heatwaves.

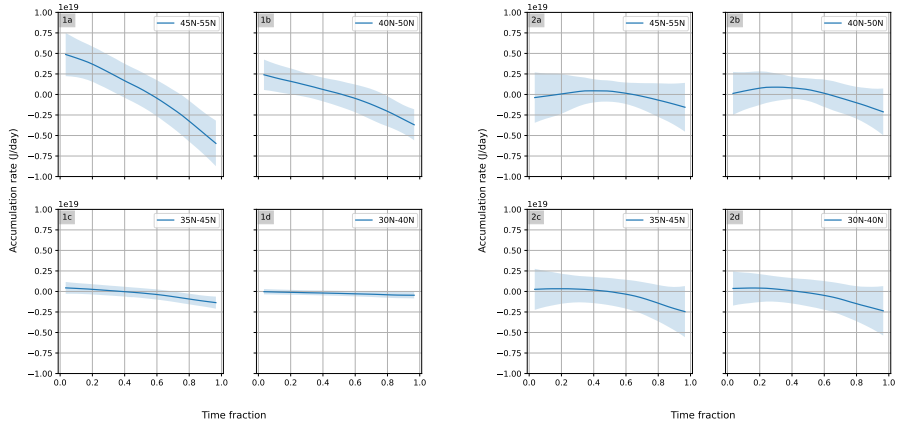

FIGURE 7 Lifetime profiles of $\overline{u}\frac{\partial S'}{\partial x}$ (1a-1d) and $u'\frac{\partial S'}{\partial x}$ (2a-2d) for high intensity heatwaves across land locations. These are plotted against time fraction, with 0 and 1 being the first and last day across heatwaves. The lines represent the mean, and shading shows standard deviation across heatwaves.

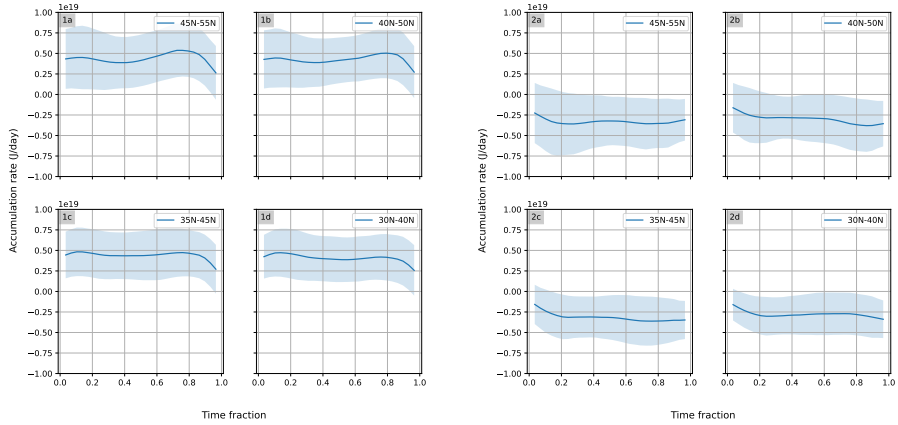

FIGURE 8 Lifetime profiles of $v' \frac{\partial \overline{S}}{\partial y}$ (1a-1d) and $v' \frac{\partial S'}{\partial y}$ (2a-2d) for high duration heatwaves across land locations. These are plotted against time fraction, with 0 and 1 being the first and last day across heatwaves. The lines represent the mean, and shading shows standard deviation across heatwaves.

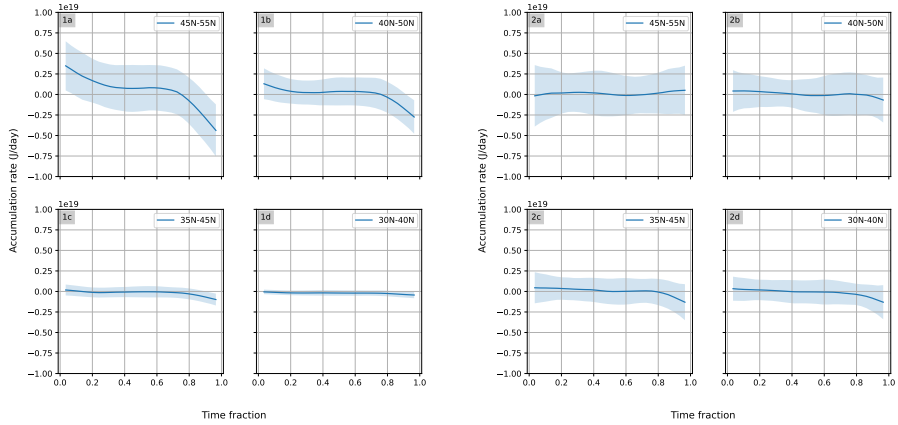

FIGURE 9 Lifetime profiles of $\overline{u}\frac{\partial S'}{\partial x}$ (1a-1d) and $u'\frac{\partial S'}{\partial x}$ (2a-2d) for high duration heatwaves across land locations. These are plotted against time fraction, with 0 and 1 being the first and last day across heatwaves. The lines represent the mean, and shading shows standard deviation across heatwaves.

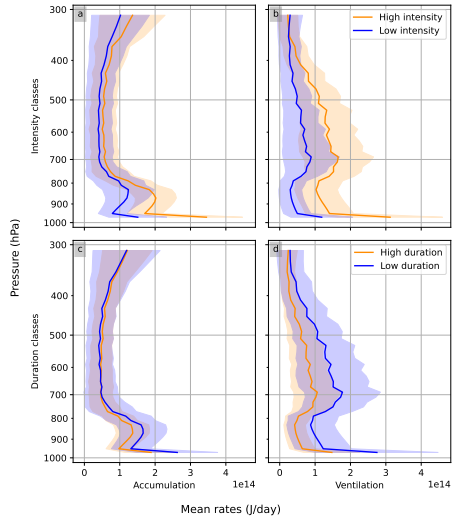

FIGURE 10 Land patch centered at 45N. Vertical profiles of mean DSE advection for the different classes of heatwaves (accumulation and ventilation plotted separately). To calculate the mean DSE accumulation profile, all instances of DSE accumulation across heatwave duration are added at each level and then divided by the heatwave duration. Similarly, the mean ventilation profile is calculated by adding up all instances of ventilation at each level and then dividing by heatwave duration. The lines represent the mean, and shading shows standard deviation across heatwaves. (a, b) high vs low intensity; (c, d) high vs low duration.

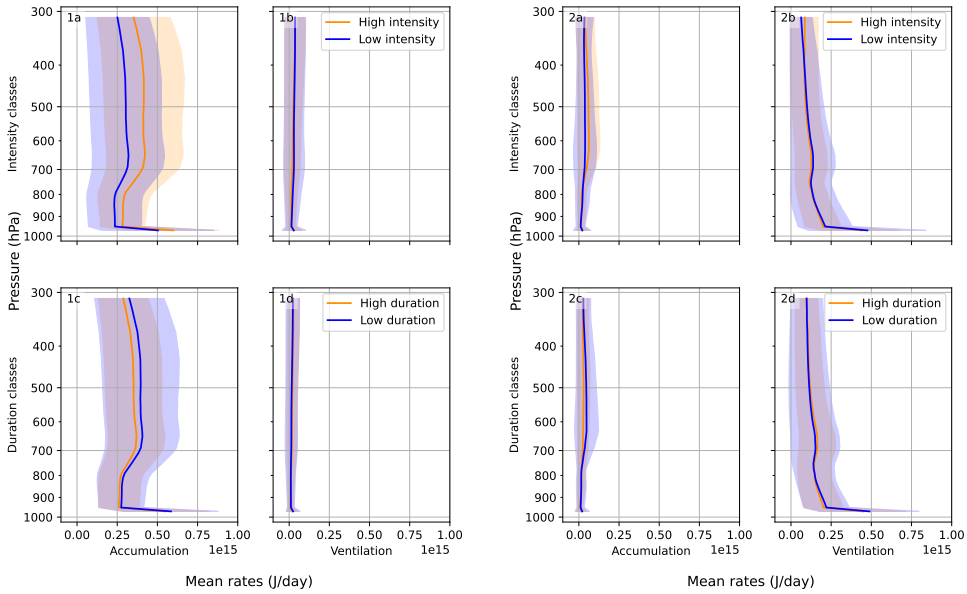

FIGURE 11 Land patch centered at 45N. The mean vertical profile of $v' \frac{\partial \overline{S}}{\partial y}$ (1a-1d) and $v' \frac{\partial S'}{\partial y}$ (2a-2d) for the the different classes of heatwaves (accumulation and ventilation plotted separately). To calculate the mean DSE accumulation profile for a component, all instances of DSE accumulation for that component across heatwave duration are added at each level and then divided by the heatwave duration. Similarly, the mean ventilation profile is calculated by adding up all instances of ventilation for a component at each level and then dividing by heatwave duration. The lines represent the mean, and shading shows standard deviation across heatwaves.

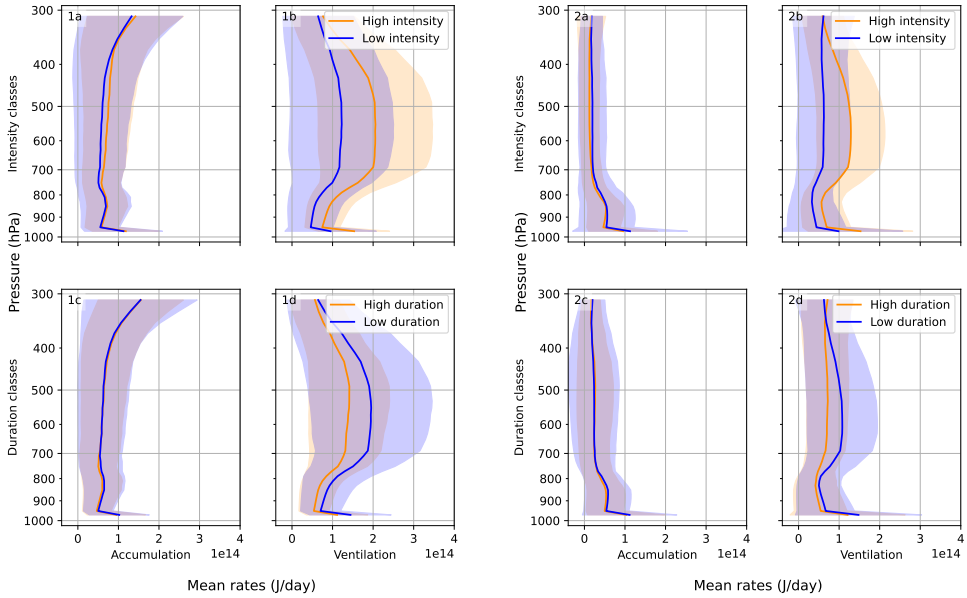

FIGURE 12 Land patch centered at 45N. The mean vertical profile of $\overline{u}\frac{\partial S'}{\partial x}$ (1a-1d) and $u'\frac{\partial S'}{\partial x}$ (2a-2d) for the the different classes of heatwaves (accumulation and ventilation plotted separately). To calculate the mean DSE accumulation profile for a component, all instances of DSE accumulation for that component across heatwave duration are added at each level and then divided by the heatwave duration. Similarly, the mean ventilation profile is calculated by adding up all instances of ventilation for a component at each level and then dividing by heatwave duration. The lines represent the mean, and shading shows standard deviation across heatwaves.

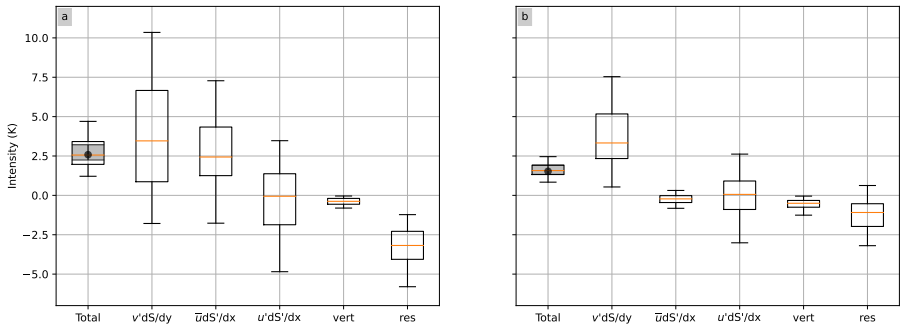

FIGURE 13 Intensity contribution of the different components for top 10 percentile intense heatwaves. The box spans from 25 to 75 percentile, and the whiskers are 5 and 95 percentile. (a) 50N patch. (b) 35N patch. "res" and "vert" are the residual and vertical terms, respectively. The shaded range overlaid on the total intensity box shows the actual intensity values of the corresponding heatwave class calculated from temperature as in Fig. 3. The shaded region spans from the 5th to the 90th percentile of heatwave intensities, with the mean intensity shown by the black dot.

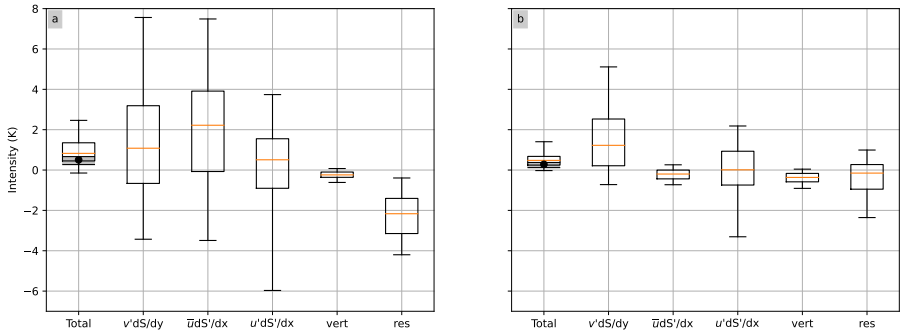

FIGURE 14 Intensity contribution of the different components for bottom 10 percentile intense heatwaves. The box spans from 25 to 75 percentile, and the whiskers are 5 and 95 percentile. (a) 50N box. (b) 35N box. res and vert are the residual and vertical terms, respectively. The shaded range overlaid on the total intensity box shows the actual intensity values of the corresponding heatwave class calculated from temperature as in Fig. 3. The shaded region spans from the 5th to the 90th percentile of heatwave intensities, with the mean intensity shown by the black dot.

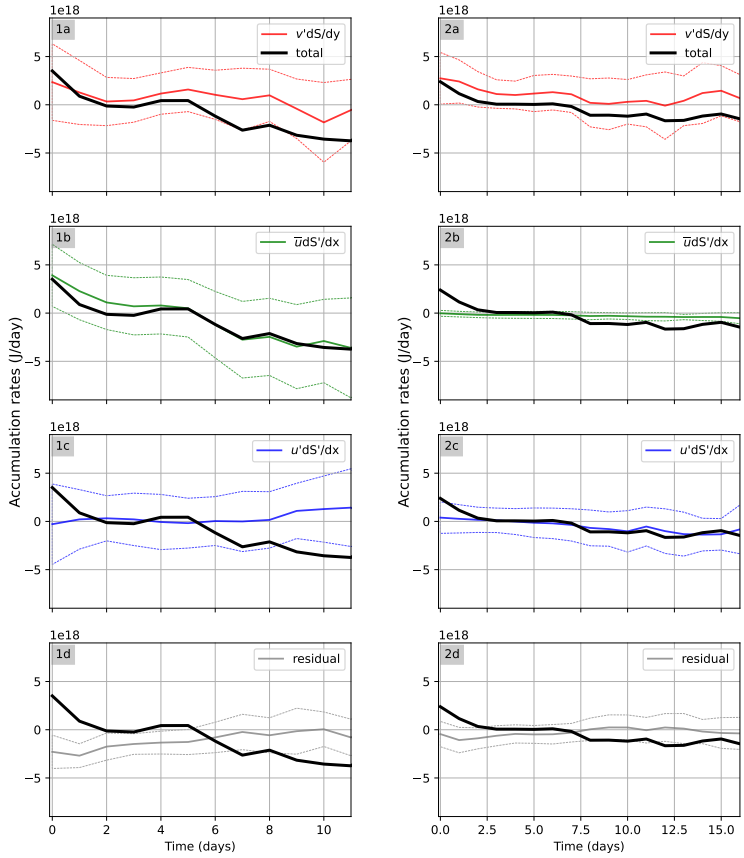

FIGURE 15 Top 10 percentile duration heatwaves. Accumulation rates associated with major components on the n^{th} day after heatwave start. The coloured solid lines are the mean profiles and the corresponding dotted lines indicate standard deviation. (1a-1d) 50N box. (2a-2d) 35N box.

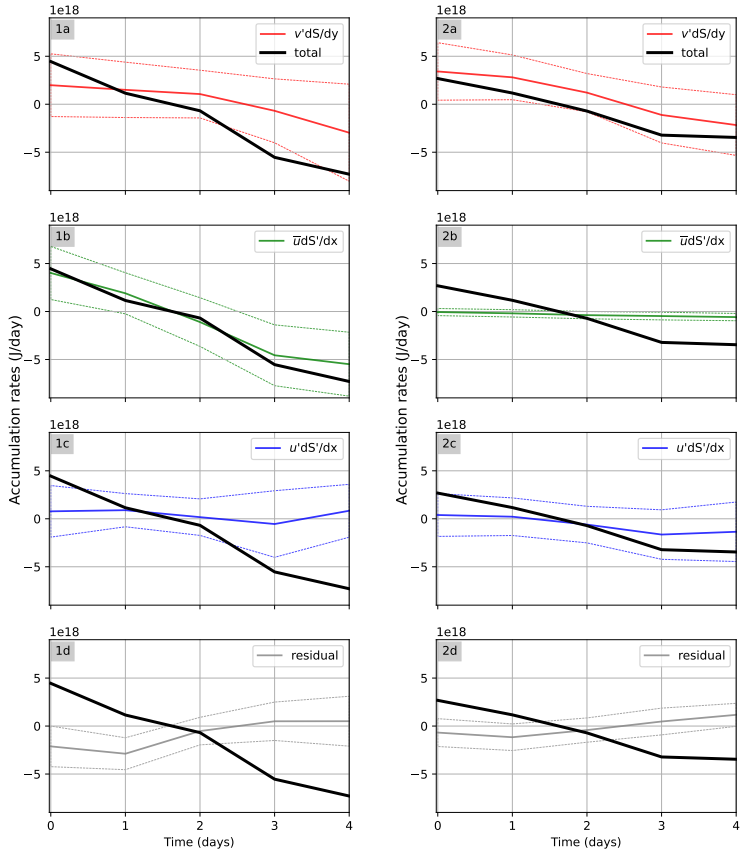

FIGURE 16 Bottom 10 percentile duration heatwaves. Accumulation rates associated with major components on the n^{th} day after heatwave start. The coloured solid lines are the mean profiles and the corresponding dotted lines indicate standard deviation. (1a-1d) 50N box. (2a-2d) 35N box.

Supplementary material

Abel Shibu[1] and Joy Monteiro[1,2]

[1]Department of Earth and Climate Science, Indian Institute of Science Education and Research Pune, Pune, India
[2]Department of Data Science, Indian Institute of Science Education and Research Pune, Pune, India

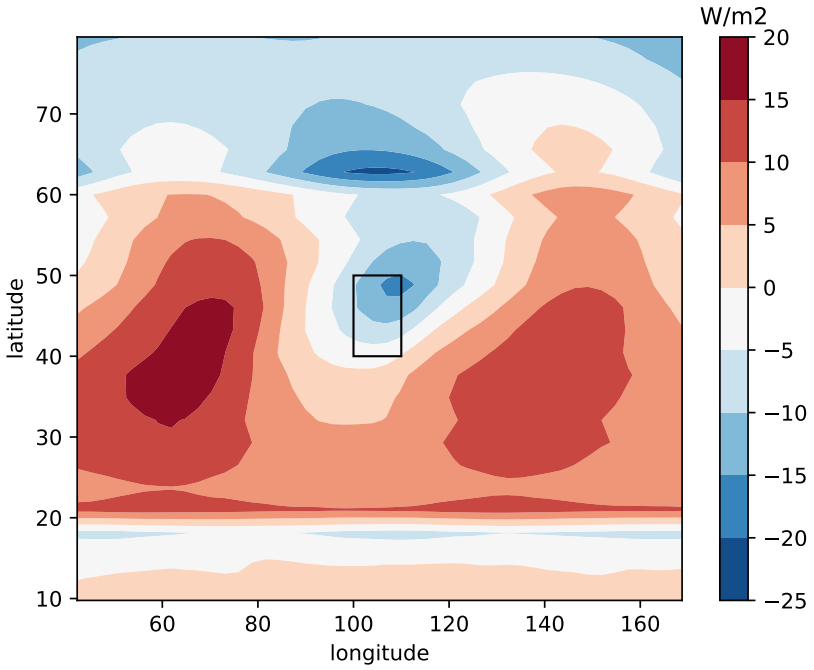

FIGURE S1: Composite of sensible heat flux anomaly at the mid-point of heat-wave duration for the land patch centered at 45N.

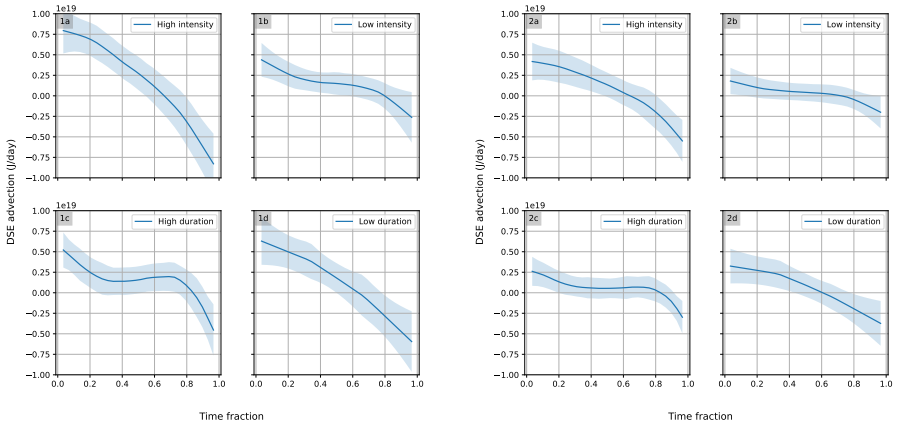

FIGURE S2: Low-level lifetime DSE advection profiles for the different intensity and duration classes reconstructed from only the four horizontal ($v'\frac{\partial \overline{S}}{\partial y}$, $v'\frac{\partial S'}{\partial y}$, $\overline{u}\frac{\partial S'}{\partial x}$ and $u'\frac{\partial S'}{\partial x}$), and the vertical components. Plots on the left (1a-1d) are for the land patch centered at 50N and plot on the right (2a-2d) are for the land patch centered at 35N. To compare between heatwaves of varying lengths, we have plotted against time fraction, with 0 and 1 being the first and last day across heatwaves. The lines represent the mean, and shading shows standard deviation across heatwaves. Left - land patch centered at 50N. Right - land patch centered at 35N.

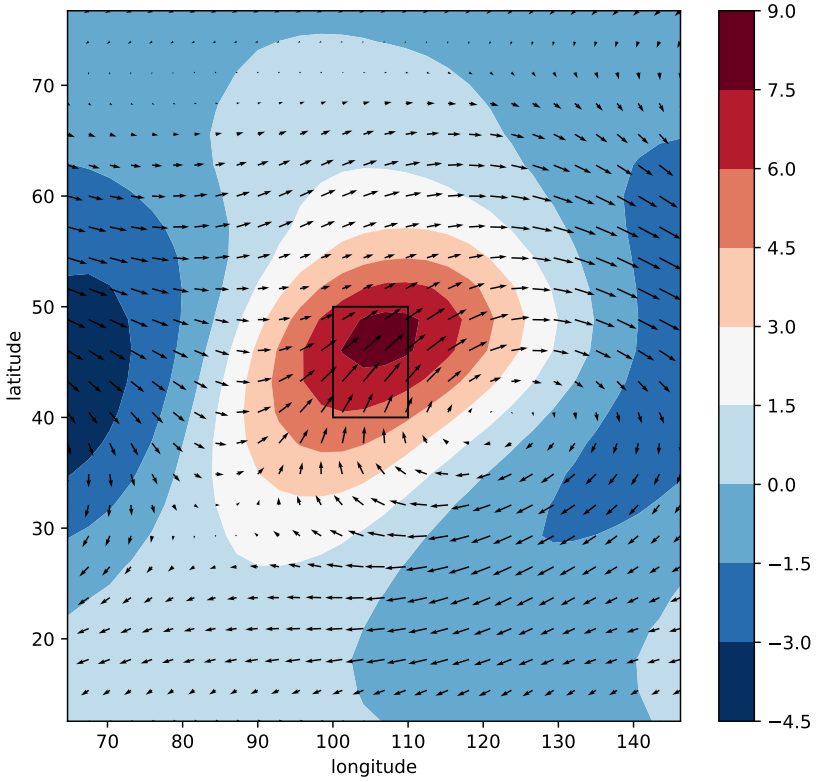

FIGURE S3: Composite plot of heatwaves at the mid-point of their duration, for the land patch centered around 45N. Lowest level winds (ms^{-1}) overlaid on lowest level air-temperature anomaly (K).

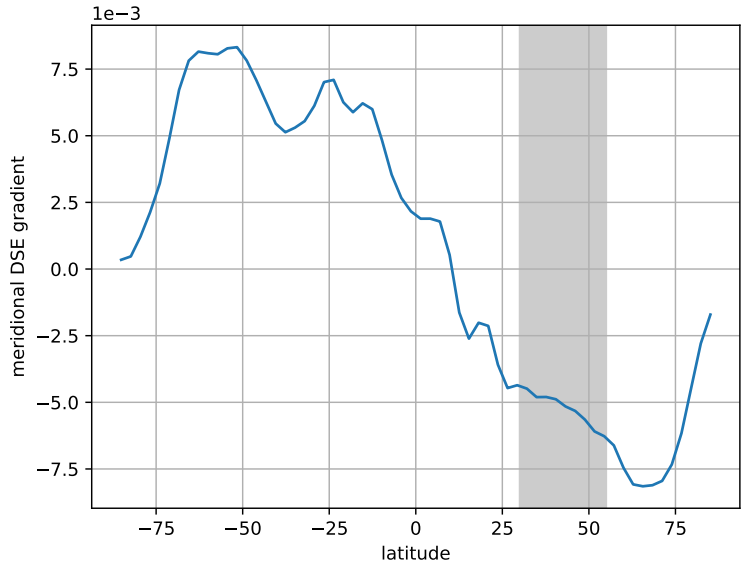

FIGURE S4: Meridional DSE gradient. The region of our study is shown by the grey shading.

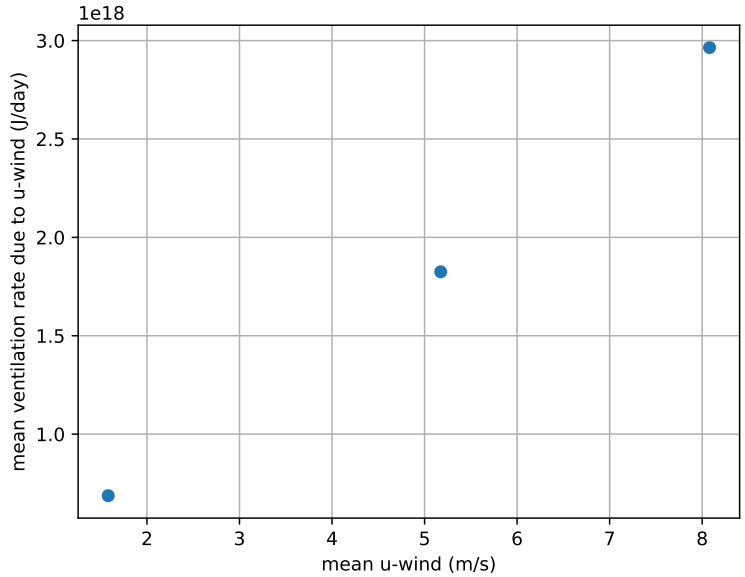

FIGURE S5: Scatter plot of average ventilation rate due to mean zonal wind during heatwaves (Jday^{-1}) vs mean zonal wind (ms^{-1}) across different land locations.